

AUTOMATED DIGITAL TOPOGRAPHIC MAPPING TECHNIQUES FOR MARS

T. Day, A.C. Cook and J-P. Muller

Department of Photogrammetry and Surveying,

University College London, Gower Street

London. WC1E 6BT, UK

e-mail: tday@ps.ucl.ac.uk, tcook@ps.ucl.ac.uk or jpmuller@ps.ucl.ac.uk

Abstract

An automated system for the production of digital elevation models from Viking Orbiter imagery has been developed by combining the Otto-Chau adaptive sheet-growing least-squares stereo-matcher and the Frankot-Chellappa shape-from-shading algorithm. Accuracy assessment results derived by comparison with manually derived photogrammetric contours from USGS Flagstaff are presented. The image selection criteria for processing large numbers of VO images is described.

Keywords: Extraterrestrial, Image Matching, Automated Mapping, Photogrammetry, Stereoscopic

1 Introduction

The EXODUS (EXtra-terrestrial Orbital DEMs for Understanding Surfaces) Project was initiated with the intention of applying automatic stereo-matching techniques developed for SPOT imagery to orbital images obtained by the Viking Orbiter probes for the purpose of constructing high resolution DEMs of Mars, including a global $\frac{1}{128}^\circ$ ($\approx 0.5\text{km}$) DEM [Muller et al. 92]. This project builds on previous work to develop an automated Digital Elevation Model (DEM) extraction system for spaceborne and industrial stereo imagery.

2 Stereo-matching

The Otto-Chau stereo-matcher [Otto and Chau, 89], and its successful application to SPOT imagery, has been documented previously in [Day and Muller, 88], [Muller, 89]. The matcher requires at least one initial seedpoint to commence sheet-growing. At the present time seed-points are generally chosen manually for each image pair to be processed, although initial experiments have been carried out with automated seedpoints based on the Foerstner operator [Allison et al. 91].

The application of the stereo-matcher to the eastern half of the South-East Aeolis mapsheet (MC-23 SE) and the Tithonium Chasma area of Valles Marineris is demonstrated.

2.1 South-East Aeolis

2.1.1 Image Selection Criteria

Viking Orbiter only had serendipitous stereo coverage as no dedicated stereo-coverage was made. In addition, al-

though most of the planet is covered with images of IFOV $\approx 250\text{m}$, only a small percentage of this area is covered with stereo at this resolution. The Mars Information System (MIS) [Cook et al. 92] was used to select the image pairs suitable for mapping of this area. The MIS holds data on the EXODUS Project's archive of 13472 Viking Orbiter images at various levels of radiometric [Batson, 87] and geometric [Edwards, 87] processing obtained from USGS Flagstaff, Goddard Space Flight Center, JPL and the University of Hawaii. We limited the number of possible pairs by applying the following chosen constraints:

Overlap The area of stereo coverage within the area of interest must be at least ten percent of the total ground area covered by the two images.

Viewing angle The spacecraft must be at least 20° above the horizon at the centre of the image.

Illumination difference The difference in solar altitude must not exceed 10° and the difference in solar azimuth must not exceed 45° (azimuth difference from [Blasius et al. 80]). We do not simply place an upper limit on the angle between illumination vectors as this could admit pairs where e.g a ridge is illuminated from opposite sides.

Resolution Ratio The ratio of image resolutions must not exceed 2.5 : 1, which appears to be the limit at which stereo matching is possible with Viking imagery and the Otto-Chau matcher.

Precision (computed as pixel IFOV divided by B/H ratio) must be better than 1km.

Camera model quality An image may have control points or good camera pointing information. There must be sufficient image navigation parameters to ensure accurate absolute orientation.

Limb Neither image must contain the limb of Mars.

Radiometric Correction At least one image of the pair must be radiometrically corrected to allow the possible application of shape-from-shading techniques.

Filter Both images must have been taken with the same colour filter in place.

Image quality A record of unuseable images is kept; this eliminates images discovered to contain e.g dust-storms, clouds and motion blur.

A search for image pairs satisfying these criteria returned 17 image pairs for the South-East Aeolis region. Selecting only image pairs in which at least one image has a resolution of 650m or better resulted in only 4 pairs.

In addition two other pairs which had lower resolution but covered a large part of the area were selected. Details of the image pairs matched are summarised in table 1.

2.1.2 Matcher Parameters

All pairs were stereo-matched using one manually selected seed-point, sheet-growing on a 4-pixel grid with a 15-pixel square patch. Constraints were:

- Maximum number of iterations = 10
- Maximum eigenvalue of translation part of variance/covariance matrix = 0.02
- Maximum absolute grey level difference between patches = twice standard deviation of left hand image
- Minimum r^2 between patches = 0.4

These parameters and constraints are based on previous experiments.

Matches were transformed to ground co-ordinates using Cook's block adjustment software [Muller et al. 92].

2.1.3 Quality Assessment

Figure 2 shows the coverage of the half-mapsheet obtained from each pair, and the statistics resulting from comparison of stereo-matcher derived elevations with the $\frac{1}{64}^\circ$ USGS DEM. A blunder is defined as a point with an absolute elevation error exceeding $3\sqrt{\sigma_a^2 + \sigma_i^2}$, where σ_a is the matcher derived estimate of the elevation accuracy and σ_i is the estimated error introduced by comparing the elevation with an interpolated surface. σ_i is computed on the assumption that USGS elevations have a standard-deviation accuracy of 0.5km, based on their contour interval of 1km.

2.1.4 Mapsheet Preparation

All matches obtained were combined using Kriging to produce a single DEM. The Kriging process requires an estimate of the variogram of the terrain being interpolated, which was obtained from the elevations derived from pair 631A58 & 639A91, which appeared to be the most blunder-free. This indicated a variance sill of 6km² at range of 1.66°; however, noise in the samples (estimated as 757m standard deviation, see Table 1) caused us to revise our estimate of the variance of the underlying terrain to 5.43km². The resulting DEM is shown in Figure 1, and should be compared with the adjacent manually derived USGS DEM. The major features show excellent agreement. The stereo-matched data shows a lot more fine structure, some of which is noise but much of which is associated with geological features, notably Ma'dim Vallis.

The Kriging process also produces a quality assurance map, shown in Figure 2. This is an estimate of the standard-deviation accuracy at each DEM grid-point, and reflects the estimated accuracy of the data from which the elevation at the grid point was interpolated, and the effect of the variogram on interpolation over a distance. The decreasing confidence caused by interpolation across holes is seen as regions of high estimated σ , and the regions

where more accurate measurements are made possible by higher resolution, higher match density or better base to height ratio pairs causes the darker areas.

On comparing the regions of our Kriged DEM for which we estimate a better than 0.5km standard-deviation error with the USGS DEM, we obtain a mean difference of 0.07km and a standard deviation difference of 0.84km. Note that we generally find Kriging to produce optimistic estimates of quality; results are worse because errors are not uncorrelated, and some blunders produce quality estimates indicating high accuracy.

2.2 Valles Marineris

The previous section showed application of the stereo-matcher to "typical" Viking stereo-pairs. Here is shown what can be achieved with higher resolution images. Unfortunately, stereo coverage at such resolutions is only available over a small proportion of the surface of Mars [Muller et al. 92].

Figure 3 shows one such high resolution image pair (details in Table 3). Figure 4 shows the DEM obtained by colleagues at the Open University [Thornhill et al. 92] using UCL's matching software, and Figure 5 the corresponding extract of the USGS DEM $\frac{1}{64}^\circ$; the differences are: $\mu = -7.377\text{km}$ and $\sigma = 1.588\text{km}$. Further analysis of the DEM obtained may be found in [Thornhill et al. 92].

3 Shape-from-Shading

Shape-from-shading is potentially useful for extracting the small-scale detail lacking in our stereo-derived DEMs. However the DEMs obtained must be treated with caution due to the errors introduced by image noise, incorrect radiometric calibration, uncertainties in the reflectance function and atmospheric effects [Jankowski and Squyres, 91].

As input we require a single radiometrically corrected image which is then ortho-projected using an inverse camera model and any available elevation information (a single representative elevation value, the USGS $\frac{1}{64}^\circ$ DEM or a stereo-matcher derived DEM). Figure 6 shows image 057A45 ortho-projected using the stereo-matched DEM from Figure 4.

3.1 Algorithm

The Frankot and Chellappa shape-from-shading algorithm [Frankot and Chellappa, 88] is used. Unlike most other published shape-from-shading algorithms, it computes a set of integrable gradients at each iteration, rather than attempting to fit a surface to a not-necessarily integrable array of gradient estimates as a post-processing operation. It is also a true surface algorithm, rather than dealing with for example: adjacent profiles or characteristic strips.

The algorithm consists of a user-specified number of iterations, each iteration includes the following steps. We start the algorithm with arrays of gradient estimates (x and y) set to zero.

- Smooth the gradient estimates using a 3x3 convolution. This step has its heritage in

Table 1: Stereo Pairs selected as being suitable for automatic mapping of SE Aeolis

Left image				Right image				Image pair		
Picno	Res.	Cam. acc.	Sol. alt.	Picno	Res.	Cam. acc.	Sol. alt.	Control points	Overlap on map	Precision
631A58	288m	SEDR	38.9°	639A91	719m	Wu	37.7°	13	36%	757m
323S57	810m	Wu	38.3°	399S01	838m	SEDR	45.2°	3	42%	863m
323S59	805m	Wu	48.3°	399S01	838m	SEDR	45.2°	14	55%	1133m
631A58	288m	SEDR	38.9°	639A92	715m	SEDR	44.1°	4	28%	895m
631A59	290m	SEDR	34.8°	639A91	719m	Wu	37.7°	5	21%	807m
631A60	294m	SEDR	40.0°	639A91	719m	Wu	37.7°	13	18%	665m

Table 2: Stereo-matcher coverage figures, and results of comparison with USGS $\frac{1}{64}$ DEM.

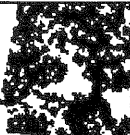
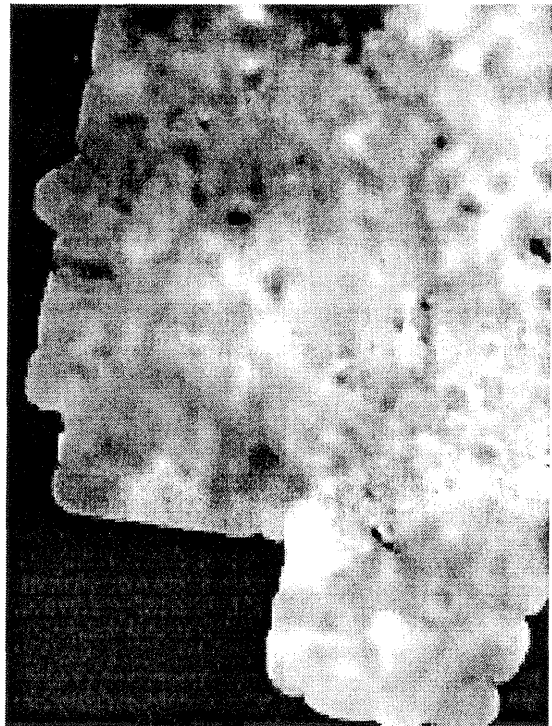
Left image	Right image	Coverage map	Difference				
			N	μ	σ	blunders	max
631A58	639A91		11929	-0.27km	0.88km	1.4%	3.63km
323S57	399S01		5331	0.32km	1.06km	7.3%	6.01km
323S59	399S01		20752	0.23km	1.20km	1.9%	32.23km
631A58	639A92		3955	-0.20km	0.75km	1.0%	5.83km
631A59	639A91		7878	0.87km	1.14km	7.8%	8.88km
631A60	639A91		14020	0.32km	1.25km	3.5%	19.64km

Figure 1: USGS $\frac{1}{32}^\circ$ DEMs of eastern half of South-East Aeolis mapsheet.

Extent: Latitude 168.75°E – 180°E, Longitude 30°S – 15°S

Intensity range images



Lambertian shaded images (illumination from East)

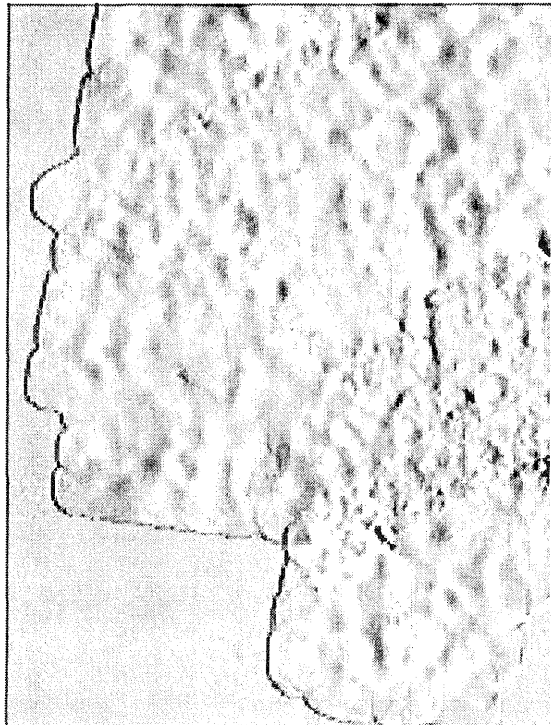
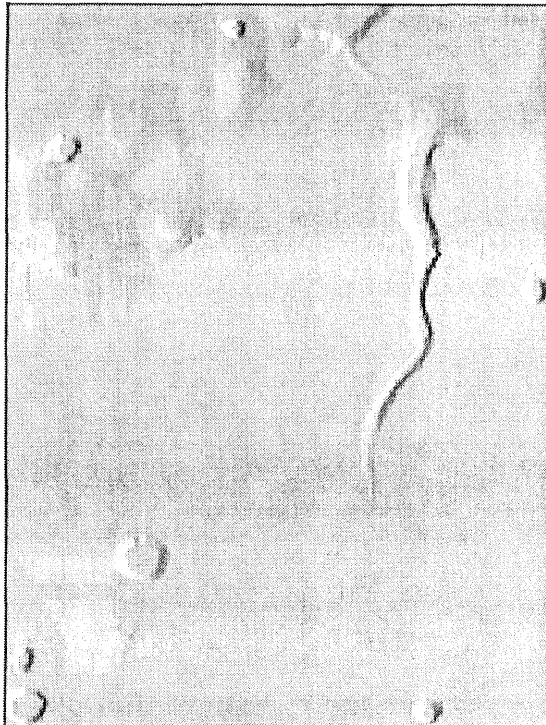


Figure 2: Estimated accuracy of Kriged DEM

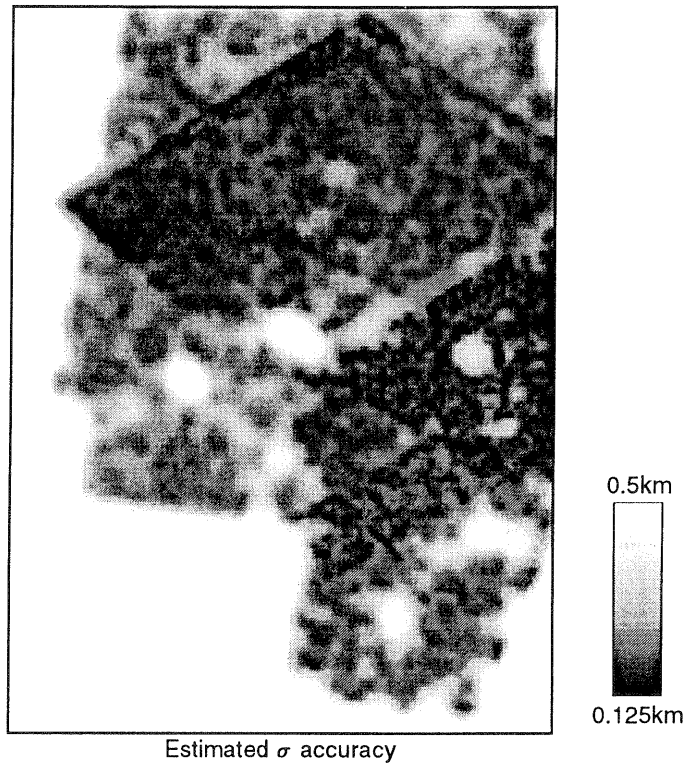


Table 3: Details of high resolution stereo pair of Valles Marineris

Left image				Right image				Image pair	
Picno	Res.	Cam. acc.	Sol. alt.	Picno	Res.	Cam. acc.	Sol. alt.	Overlap	Precision
057A45	108m	Wu	61.3°	064A22	78m	SEDR	61.5°	47%	227m

Figure 3: Image pair 057A45 & 064A22

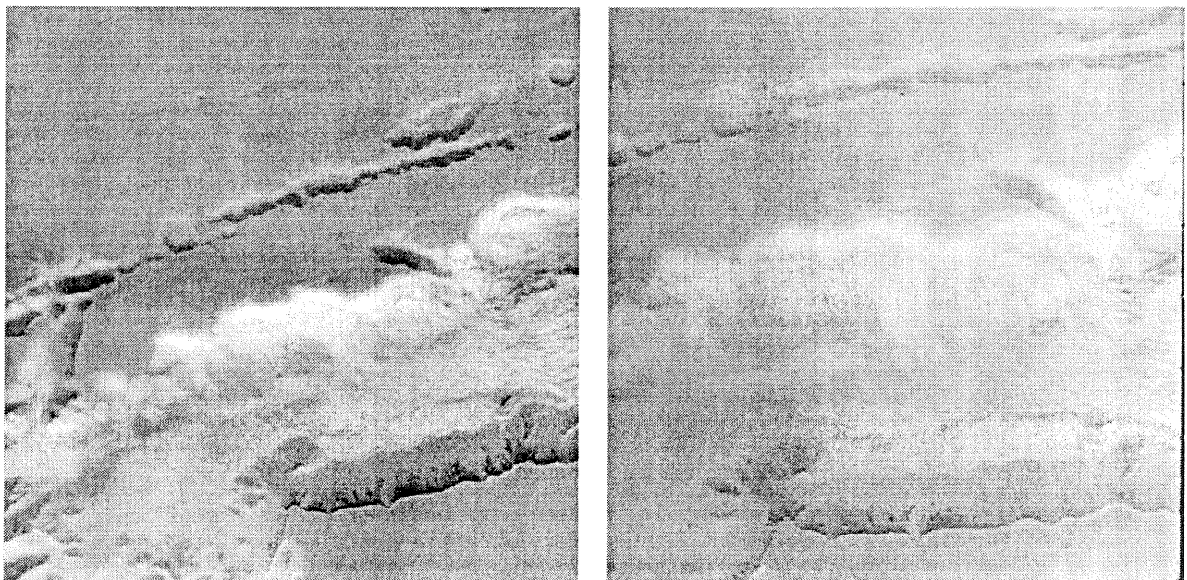


Figure 4: Stereo-matcher derived DEM of Valles Marineris

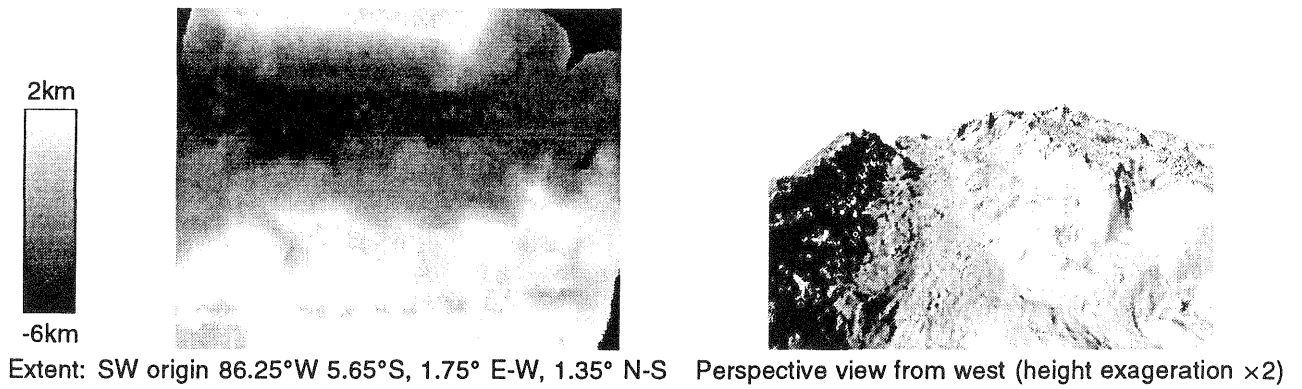


Figure 5: USGS DEM of Valles Marineris

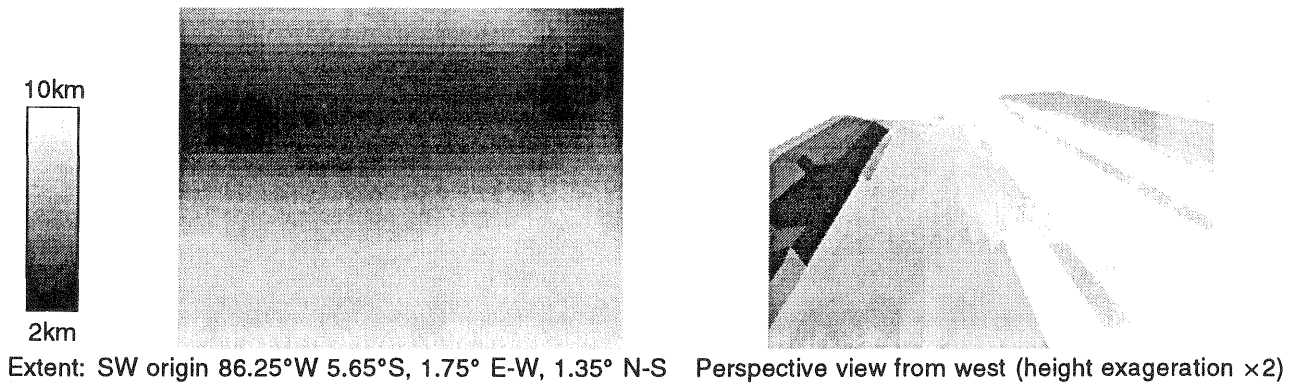
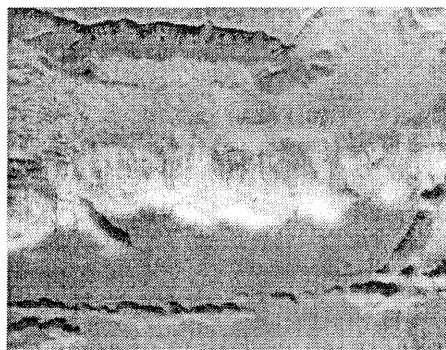


Figure 6: Orthoimage of Valles Marineris



Resampled from image 057A45
Extent: SW origin 86.25°W 5.65°S, 1.75° E-W, height 1.35° N-S

[Horn and Brooks, 86] where it is required for convergence. However, in our experience it is not necessary in the Frankot-Chellappa algorithm applied to Mars or SPOT imagery.

- Improve each of the gradient estimates independently by adjusting them towards the value minimising the difference between observed and computed (from the gradients) intensity. The algorithm's λ parameter controls the rate of adjustment.
- Project the gradients to an integrable surface, minimising the sum of the squares of the adjustments required. This is done in Fourier space.

The periodic wrap-round nature of the discrete Fourier transform representation results in distortions at opposite edges of the DEM. We overcome this by padding the image to double size with a uniform grey-level equal to that produced by a flat surface.

[Frankot and Chellappa, 88] used a central-differencing differentiation operator. This results in a slightly corrugated appearance to the output DEM, as central differencing cannot "see" corrugations. We obtain stripe-free output using forward differencing.

3.2 Calibration

Given a radiometrically corrected Viking Orbiter image we must still account for the effects of surface reflectance and atmospheric scattering. Two numbers are required to effect a linear transformation between image grey levels and the normalised range used internally. We currently specify the "shadow current" and the "flat current". The shadow current is the grey level with which a self-shadowed slope will appear in the image; we generally estimate this to be equal to the darkest pixel in the resseau-removed image (N.B This is not equivalent to the camera's "dark current", which would not compensate for atmospheric scattering). The flat current is the grey level with which a level piece of terrain will appear; we estimate this from the modal grey-level in the scene. We believe this to be appropriate as most of the scenes to which we have applied shape-from-shading have contained large apparently flat areas of almost uniform grey-level.

Errors in calibration generally result in long-range curvature of the output DEM. We can compensate for this to an extent by adjusting the calibration parameters in order to eliminate long-range elevation trends. In future we expect to make use of information such as the USGS DEM.

Figure 7 shows the DEM obtained by applying shape-from-shading to an extract from the orthoimage in figure 6. A Minnaert reflectance function with parameter 0.85 (compatible with [Davis and Soderblom, 84], given the 53.2° phase angle for this image) was assumed. The corresponding extract of the stereo-matched DEM is also shown as a perspective view; the sloping terrain feature may correspond to the eastern crater wall, but overall there is little resemblance to a crater unlike the shape from shading results. In future it is hoped to be able to replace selected areas of stereo-matched DEM containing higher frequencies with the shape-from-shading derived elevation models containing higher frequency intervals.

4 Conclusions

While matching techniques developed for SPOT do seem to be applicable to Viking Orbiter, the resolution of the imagery available over most of the Martian surface permits only extraction of the largest terrain features. Shape from shading offers a way of extracting features such as craters in some regions.

In the near future, combined use of the existing USGS DEM with the images available may permit global coverage to be achieved even given the poor stereo coverage of Viking Orbiter. Longer term, the Mars Observer Laser Altimeter coupled with the MO camera and the HDSC on Mars 94 will permit these techniques to be more fully exploited.

5 Acknowledgements

The EXODUS project is supported by SERC grants GR/F-84-294 and GR/F-82-894 jointly with David Rothery, John Murray and Gillian Thornhill at the Department of Earth Sciences, Open University. We would like to thank Sherman Wu, Debbie Cook, Kay Edwards and Annie Howington at USGS Flagstaff for all their help and support and Sue MacMahon at JPL.

References

- D Allison, M J A Zemerly, and J-P Muller (1991). Automatic Seed Point Generation for Stereo Matching and Multi-Image Registration. In *Proceedings International Geoscience and Remote Sensing Symposium, Helsinki, Finland (IEEE Catalogue 91CH2971-0)*, June 1991.
- R Batson (1987). Digital Cartography of the Planets: New Methods, Its Status and Its Future. *Photogrammetric Engineering and Remote Sensing*, 53(9):1211-1218, 1987.
- K R Blasius, A V Vetrone, and M D Martin (1980). Viking Orbiter Stereo Imaging Catalog. NASA Contractor Report 3277, NASA, June 1980.
- A C Cook, T Day, J C Iliffe, and J-P Muller (1992). A Prolog-Based Mars Information System. In *International Archives of Photogrammetry and Remote Sensing*, 1992. WG IV/6.
- P A Davis and L A Soderblom (1984). Modeling Crater Topography and Albedo from Monoscopic Viking Orbiter Images. *Journal of Geophysical Research*, 89(B11):9449-9457, October 1984.
- T Day and J P Muller (1999). Quality Assessment of Digital Elevation Models Produced by Automatic Stereomatchers from SPOT Image Pairs. *Photogrammetric Record*, 12(72):797-808, October 1988.
- K Edwards (1987). Geometric Processing of Digital Images of the Planets. *Photogrammetric Engineering and Remote Sensing*, 53(9):1219-1222, 1987.

R T Frankot and R Chellappa (1988). A Method for Enforcing Integrability in Shape from Shading Algorithms. *IEEE Transactions on Pattern Analysis and Machine Intelligence*, 10(4):439-451, July 1988.

B K P Horn and M J Brooks (1986). The Variational Approach to Shape from Shading. *Computer Vision, Graphics and Image Processing*, 33:174-208, February 1986.

D G Jankowski and S W Squyres (1991). Sources of Error in Planetary Photoclinometry. *Journal of Geophysical Research*, 96(E4):20907-20922, November 1991.

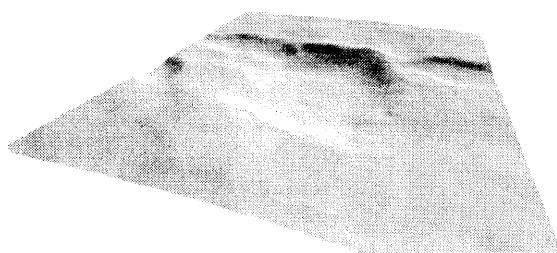
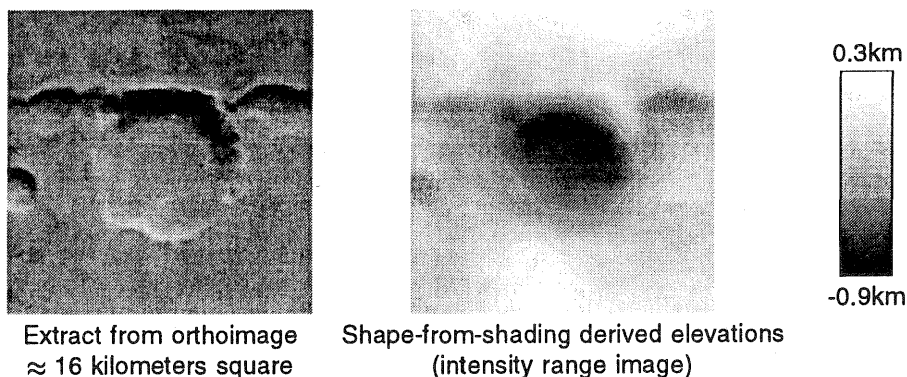
J-P Muller (1989). Real-Time Stereo Matching and Its Role in Future Mapping Systems. In *Survey & Mapping 89. University of Warwick. 17-21 April, 1989.*

J-P Muller, A C Cook, T Day, and J C Iliffe (1992). Global topography of Mars from Automated Image Understanding of Viking Orbiter Data. In *International Archives of Photogrammetry and Remote Sensing*, 1992. WG IV/6.

G P Otto and T K W Chau (1989). A "Region-Growing" Algorithm for Matching of Terrain Images. *Image & Vision Computing*, 7(2):83-94, May 1989.

G D Thornhill, J B Murray, D A Rothery, T Day, A C Cook, J Iliffe, and J-P Muller (1992). Comparison of Automatically Generated Digital Elevation Model of Tithonium Chasma with USGS Interpolated Contour Digital Elevation Model. In *23rd Lunar and Planetary Science Conference, Johnson Space Center, Houston, Texas, March 1992.*

Figure 7: Shape from shading output



Visualisation of DEM obtained



Visualisation of corresponding area of stereo-matched DEM